

Mott-Hubbard gap closure and structural phase transition in the oxyhalides TiOBr and TiOCl under pressure

C. A. Kuntscher,* A. Pashkin, H. Hoffmann, S. Frank, M. Klemm, and S. Horn
Experimentalphysik 2, Universität Augsburg, D-86135 Augsburg, Germany

A. Schönleber and S. van Smaalen
Laboratory of Crystallography, Universität Bayreuth, 95440 D-Bayreuth, Germany

M. Hanfland
European Synchrotron Radiation Facility, BP 220, F-38043 Grenoble, France

S. Glawion, M. Sing, and R. Claessen
Experimentelle Physik 4, Universität Würzburg, 97074 D-Würzburg, Germany
 (Dated: August 30, 2021)

Pressure-dependent transmittance and reflectance spectra of TiOBr and TiOCl single crystals at room temperature suggest the closure of the Mott-Hubbard gap, i.e., the gap is filled with additional electronic states extending down to the far-infrared range. According to pressure-dependent x-ray powder diffraction data the gap closure coincides with a structural phase transition. The transition in TiOBr occurs at slightly lower pressure ($p=14$ GPa) compared to TiOCl ($p=16$ GPa) under hydrostatic conditions, which is discussed in terms of the chemical pressure effect. The results of pressure-dependent transmittance measurements on TiOBr at low temperatures reveal similar effects at 23 K, where the compound is in the spin-Peierls phase at ambient pressure.

PACS numbers:

I. INTRODUCTION

The layered compounds TiOX, where $X=Br$ or Cl , are low-dimensional systems which show interesting magnetic and electronic properties. Regarding the spin degree of freedom, at high temperature the system can be well described by a one-dimensional spin-1/2 nearest-neighbor Heisenberg model with a Bonner-Fisher type magnetic susceptibility.^{1,2} Below the transition temperature T_{c1} , where $T_{c1}=27$ K for TiOBr and $T_{c1}=67$ K for TiOCl, TiOX undergoes a first-order phase transition to a spin-Peierls state with a dimerization of the chains of Ti atoms along the b axis and a doubling of the unit cell.^{1,3,4} Furthermore, an intermediate phase for the temperature range $T_{c1}<T<T_{c2}$ was found (with $T_{c2}=47$ K for TiOBr and $T_{c2}=91$ K for TiOCl), whose nature is now well established as an incommensurately modulated structure with a one-dimensional modulation in monoclinic symmetry.⁵ Regarding the charge degree of freedom, the Ti ions have the electronic configuration $3d^1$. The $3d$ electrons are localized due to strong electronic correlations, and hence TiOBr and TiOCl are Mott-Hubbard insulators, with a charge gap of ≈ 2 eV.^{6,7,8} It was predicted that these materials exhibit a resonating valence bond state and high-temperature superconductivity upon doping.^{9,10} However, up to now a metallization of TiOX upon doping could not be achieved.¹¹

Recently it was shown that the optical response of both compounds changes drastically under pressure: Above a critical pressure, the transmittance is suppressed and the reflectance increases in the infrared range. The changes could be attributed to additional electronic states fill-

ing the Mott-Hubbard gap and they suggest a closure of the gap at elevated pressures.^{7,8} Under hydrostatic conditions the transition pressures are 14 and 16 GPa for TiOBr and TiOCl, respectively. Concurrent with the closure of the Mott-Hubbard gap a structural phase transition is observed.⁸

This paper is a follow-up of the earlier, short publication⁸ and provides details of the changes in the electronic properties and crystal structure of TiOBr and TiOCl induced by external pressure. The manuscript is organized as follows: After describing the experimental details in Sec. II, we present in Sec. III A the experimental results obtained at room temperature, which suggest the closure of the Mott-Hubbard gap under pressure. We also include low-temperature transmittance spectra of TiOBr at ambient and high pressure in Sec. III B. Sec. III C focuses on the pressure-induced changes of the crystal structures for TiOBr and TiOCl. In Sec. IV A we comment about a possible chemical pressure effect in the system TiOX. In Sec. IV B the relation between the closure of the Mott-Hubbard gap and the structural phase transition is discussed. Finally, we summarize our results in Sec. V.

II. EXPERIMENT

Single crystals of TiOX ($X=Br,Cl$) were synthesized by chemical vapor transport technique. The TiOX compounds crystallize in the space group $Pm\bar{m}n$ at ambient conditions and consist of distorted TiO_4X_2 octahedra.^{12,13} The octahedra are arranged such that

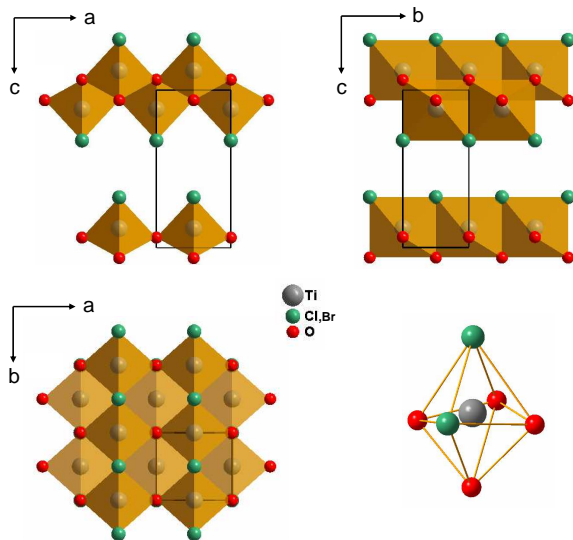


FIG. 1: Crystal structure of TiOX ($X=\text{Br,Cl}$), viewed along the a , b , and c crystal axes, consisting of Ti-O bilayers parallel to the ab -plane and separated by layers of X ions stacked along the c direction.¹² The black lines mark the unit cell. Also shown is the main building block of the crystal structure, namely the distorted TiO_4X_2 octahedron.

buckled Ti-O bilayers parallel to the ab -plane are formed, which are separated by layers of Br/Cl ions stacked along the c direction. Fig. 1 shows the crystal structure viewed along the crystal axes a , b , and c . TiOX crystals grow in the form of thin platelets with the surface parallel to the ab -plane. This is convenient for studies of the optical response of the ab -plane.

In the pressure-dependent studies diamond anvil cells (DACs) were used for the generation of pressures. The applied pressures p were determined with the ruby luminescence method.¹⁴ For the transmittance measurements several pressure transmitting media were used; this leads to small differences in the observed values of the critical pressure of phase transition, as expected.^{7,15} For the reflectance measurements finely ground CsI powder was chosen as pressure medium to insure direct contact of the sample with the diamond window.

Pressure-dependent transmittance and reflectance experiments were conducted at room temperature using a Bruker IFS 66v/S FT-IR spectrometer with an infrared microscope (Bruker IRscope II). For the generation of pressure we used a Syassen-Holzapfel DAC¹⁶ equipped with type IIA diamonds suitable for infrared measurements. Part of the measurements were carried out at the infrared beamline of the synchrotron radiation source ANKA, where the same equipment is installed. Further information on the pressure-dependent transmittance and reflectance measurements conducted at room temperature was included in the earlier publication.⁸

For TiOBr the transmittance measurements under pressure were also conducted at 23 K for the frequency range $3100 - 15000 \text{ cm}^{-1}$ (0.38 - 1.9 eV). At 23 K TiOBr

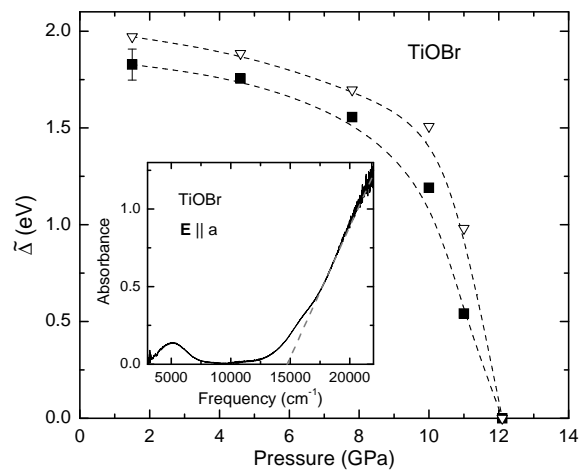


FIG. 2: Charge gap $\tilde{\Delta}$ (see text for definition) of TiOBr as a function of pressure for $\mathbf{E}||a$ (full symbols) and $\mathbf{E}||b$ (open symbols) (pressure medium: CsI). The dashed lines are guides to the eye. Inset: Absorbance spectrum $A(\omega)$ of TiOBr for the lowest pressure (1.5 GPa), calculated according to $A(\omega)=\log_{10}[1/T(\omega)]$, together with the linear extrapolation of the absorption edge (dashed gray line) used to estimate $\tilde{\Delta}$.

is in the spin-Peierls phase at ambient pressure. As pressure medium argon was used. The transmittance measurements on the sample in the DAC placed in the optical cryostat (CryoVac KONTI cryostat) were performed using a home-built infrared microscope with a large working distance. This infrared microscope can be directly coupled to the FT-IR spectrometer and maintained at the same pressure ($\approx 3 \text{ mbar}$), i.e., no window between the two devices is needed.

Pressure-dependent x-ray powder diffraction measurements at room temperature were carried out at beamline ID09A of the European Synchrotron Radiation Facility at Grenoble. Details about the experiments were described elsewhere (Ref.8).

III. RESULTS AND ANALYSIS

A. Pressure-dependent transmittance and reflectance at room temperature

Pressure-dependent transmittance measurements on TiOBr and TiOCl were carried out for several pressure transmitting media. In Refs.7,8 we already showed the spectra of TiOBr and TiOCl for argon and CsI as pressure media, respectively. The transmittance spectra reveal the characteristic excitations in the materials, namely the electronic transitions between the lower and upper Hubbard gap, resulting in a strong suppression of the transmittance above $\approx 2 \text{ eV}$. Furthermore, absorptions occur due to excitations across the crystal-field split $\text{Ti}3d$ energy levels (called orbital excitations in the following) located for TiOBr (TiOCl) at 0.63 eV (0.66 eV)

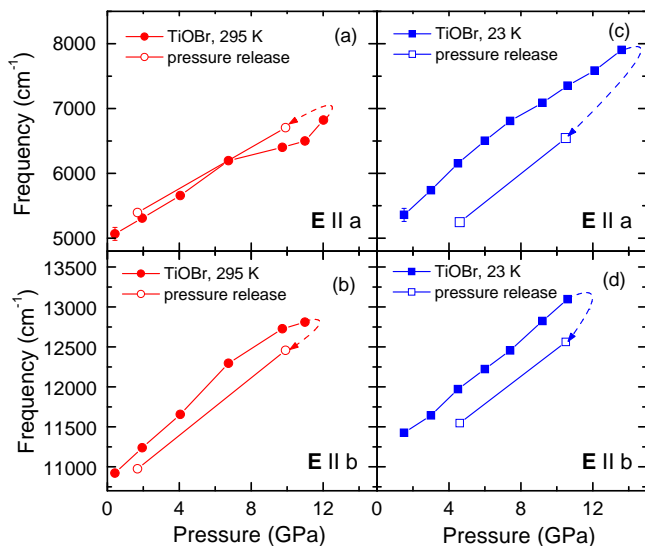


FIG. 3: (Color online) Frequency of the orbital excitations in TiOBr as a function of pressure: at room temperature for the polarization (a) $\mathbf{E}||a$ and (b) $\mathbf{E}||b$; at 23 K for the polarization (c) $\mathbf{E}||a$ and (d) $\mathbf{E}||b$ (pressure medium: argon). The full symbols denote the results with increasing pressure; open symbols denote the results upon pressure release. Lines are guides to the eye.

for $\mathbf{E}||a$ and at 1.35 eV (1.53 eV) for $\mathbf{E}||b$ at ambient conditions.

First, one notices that in TiOBr the orbital excitations are slightly redshifted compared to TiOCl. This can be explained by the chemical pressure effect in the system TiOX : Based on the g tensors measured by electron spin resonance²⁰ the crystal field splittings in TiOBr and TiOCl were obtained. The smaller crystal field splitting in TiOBr could be attributed to the larger size of the Br^- ion compared to the Cl^- ion, causing a larger volume of the TiO_4X_2 octahedra (see Fig. 1) and hence a weaker crystal field.²⁰

With increasing pressure one observes the following changes for both compounds along the two studied polarization directions: (i) a blueshift of the orbital excitations; (ii) the absorption edge due to excitations across the charge gap shifts to smaller energies with increasing pressure, and above 11 GPa (12 GPa) the overall transmittance is strongly suppressed in TiOBr (TiOCl). These results were obtained with CsI as pressure medium; when a more hydrostatic pressure medium is used (see Table I and the results in Ref. 8), the suppression of the transmittance occurs at somewhat higher pressure ($\Delta p \approx 4$ GPa).

We estimated the charge gap, $\tilde{\Delta}$, by a linear extrapolation of the steep absorption edge. This is illustrated in the inset of Fig. 2, where we show the absorbance spectrum $A(\omega)$ of TiOBr for the lowest pressure (1.5 GPa), calculated from the transmittance $T(\omega)$ according to $A(\omega) = \log_{10}[1/T(\omega)]$, together with the linear extrapolation of the absorption edge. The intersection of the

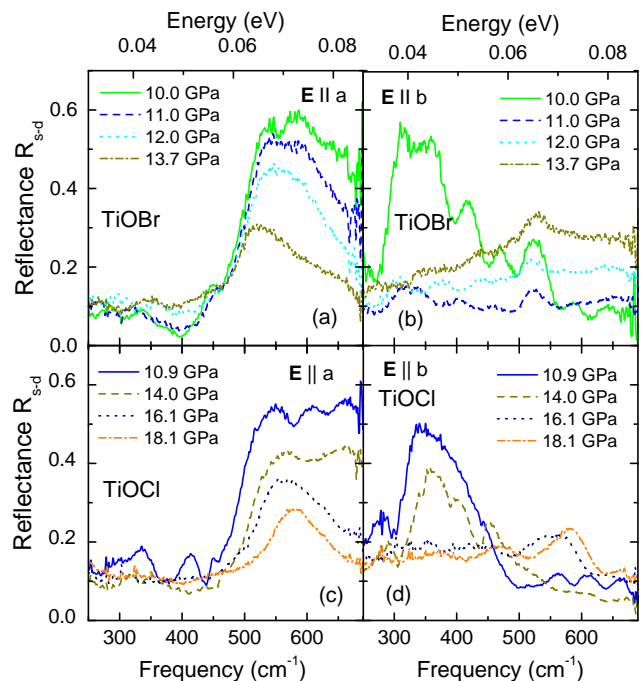


FIG. 4: (Color online) Far-infrared reflectance R_{s-d} of TiOBr and TiOCl at room temperature as a function of pressure, for the polarization $\mathbf{E}||a$ [(a) and (c), resp.] and $\mathbf{E}||b$ [(b) and (d), resp.] (pressure medium: CsI).

linear extrapolation with the horizontal axis was taken as an estimate of the charge gap. Starting from the lowest applied pressure, $\tilde{\Delta}$ initially slightly decreases with increasing pressure, and above ≈ 10 GPa it rapidly drops to zero (Fig. 2). Similar observations were made earlier for TiOCl,⁷ with the onset of rapid decrease of $\tilde{\Delta}$ at $p \approx 12$ GPa.

The pressure dependence of the frequencies of the orbital excitations in TiOBr were obtained by fitting the absorption features in the transmittance spectra with Gaussian functions. The results are depicted in Fig. 3. With increasing pressure the orbital excitations shift to higher frequencies in a linear fashion. This shift could be attributed to a monotonically increasing strength of the crystal field related to the decreasing volume of the TiO_4Br_2 octahedra. External pressure could also induce a change in the octahedral distortion and related alterations of the crystal field. One furthermore notices a small difference in the frequency of the orbital excitations for pressure increase and decrease observed in the direction $\mathbf{E}||b$ [Fig. 3(b)], which suggests that the pressure-induced octahedral volume decrease and/or octahedral distortion are not completely reversible. This non-reversibility is more obvious at low temperatures and will be discussed in Sec. III B.

Additional information about the pressure-induced changes in the optical response were obtained by reflectance measurements on TiOBr and TiOCl at high pressures. The most drastic changes occur in the far-

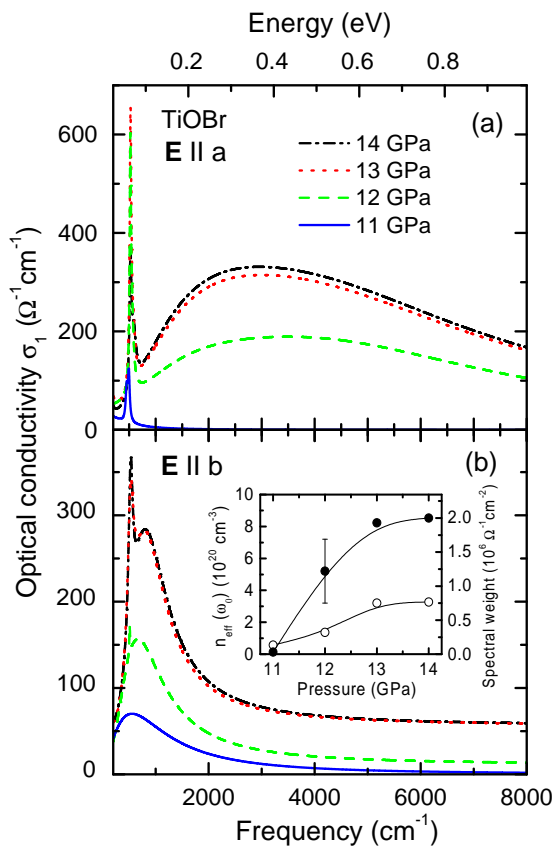


FIG. 5: (Color online) Real part of the optical conductivity of TiOBr as a function of pressure for the polarization (a) $\mathbf{E}||a$ and (b) $\mathbf{E}||b$ obtained by Drude-Lorentz fitting of the pressure-dependent reflectance data R_{s-d} . Inset: Total effective carrier density, n_{eff} , and spectral weight calculated by integrating the real part of the optical conductivity (see text) up to $\omega_0=8000 \text{ cm}^{-1}$ for $\mathbf{E}||a$ (filled circles) and $\mathbf{E}||b$ (open circles). Lines are guides to the eye.

infrared range, as illustrated for both compounds in Figs. 4 (a) and (b) (for pressure-dependent reflectance spectra over a broader frequency range, see Refs.7,8). In case of TiOBr, the shape of the spectrum changes drastically for $\mathbf{E}||b$: At 10 GPa the spectrum consists of a peak-like feature between 300 and 450 cm^{-1} , whereas for pressures ≥ 11 GPa it is almost flat with a peak at around 520 cm^{-1} . The pressure-induced changes in the far-infrared reflectance spectra R_{s-d} of TiOCl are very similar to those of TiOBr [see Figs. 4 (c) and (d)]. However, for TiOCl the changes occur at somewhat higher pressure, as discussed in Sec. IV A. For higher frequencies the overall reflectance increases for both compounds and saturates.^{7,8}

The suppression of the transmittance in TiOX at high pressures suggests the occurrence of new excitations in the infrared frequency range. More information about these additional excitations were obtained by fitting the high-pressure ($p > 10$ GPa) reflectance spectra R_{s-d} with the Drude-Lorentz model combined with the

normal-incidence Fresnel equation, taking into account the diamond-sample interface:

$$R_{s-d} = \left| \frac{n_{\text{dia}} - \sqrt{\epsilon_s}}{n_{\text{dia}} + \sqrt{\epsilon_s}} \right|^2, \quad \epsilon_s = \epsilon_\infty + \frac{i\sigma}{\epsilon_0\omega}, \quad (1)$$

where ϵ_s is the complex dielectric function of the sample and ϵ_∞ is the background dielectric constant (here $\epsilon_\infty \approx 3$). From the function $\epsilon_s(\omega)$ the real part of the optical conductivity, $\sigma_1(\omega)$, can be calculated. Notice that only reflectance data above 10 GPa can be analyzed quantitatively because of the partial transparency of the sample below this critical pressure.

The evolution of the optical conductivity of TiOBr with pressure is shown in Fig. 5. We find additional excitations in the infrared range, extending down to the far-infrared. These additional excitations include broad excitations, which cannot be attributed to phonon excitations, in contrast to the optical conductivity spectrum in the insulating phase.²¹ Thus, the Mott-Hubbard gap is gradually filled with additional electronic states down to at least 200 cm^{-1} (24 meV). This finding suggests the closure of the Mott-Hubbard gap above $p=10$ GPa.

With increasing pressure the spectral weight of the pressure-induced features increases, with a saturation setting in at around 13 GPa. From the spectral weight analysis one can extract the effective density of carriers, n_{eff} , involved in the excitations up to ω_0 according to

$$n_{eff}(\omega_0) = (2m_0/\pi e^2) \int_0^{\omega_0} \sigma_1(\omega) d\omega, \quad (2)$$

with the free electron mass, m_0 . In the inset of Fig. 5(b) $n_{eff}(\omega_0=8000 \text{ cm}^{-1})$ is plotted as a function of pressure p . $n_{eff}(p)$ illustrates the saturation of the spectral features at high pressures.

Also for TiOCl the spectral weight of the pressure-induced excitations increases with increasing pressure and saturates, as presented in the earlier publication.⁷ The saturation, however, happens at somewhat higher pressure (≈ 15 GPa) compared to TiOBr. In fact, all the pressure-induced effects occur in TiOCl at slightly higher pressures ($\Delta p \approx 2$ GPa) compared to TiOBr. This pressure difference will be discussed in more detail in Sec. IV A.

B. Pressure-dependent transmittance of TiOBr at low temperatures

We have furthermore checked the stability of the insulating spin-Peierls phase of TiOBr by pressure-dependent transmittance measurements at low temperatures in the near-infrared frequency range (3100 - 15000 cm^{-1}). As mentioned in the introduction, TiOBr undergoes two phase transitions as a function of temperature: Upon temperature increase, a first order transition takes place at $T_{c1}=27$ K from the spin-Peierls ground state into an intermediate phase with an incommensurate

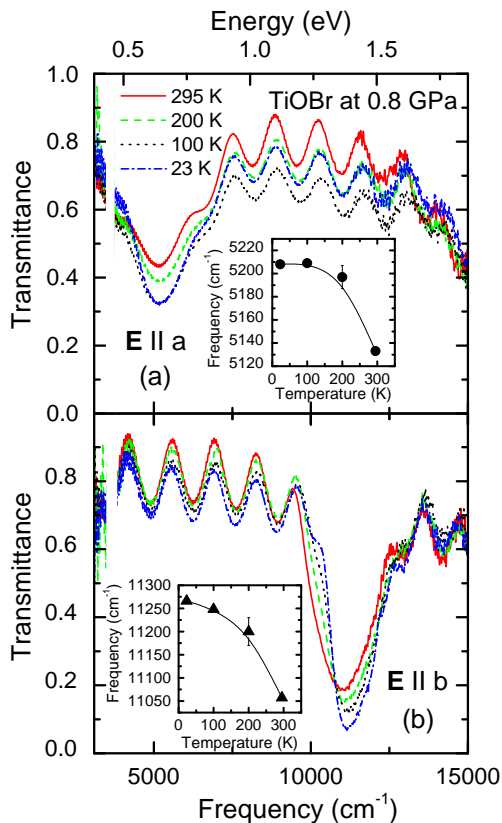


FIG. 6: (Color online) Transmittance $T(\omega)=I_s(\omega)/I_r(\omega)$ (see text for definitions) of TiOBr as a function of temperature for the lowest pressure (0.8 GPa), for the polarization (a) $\mathbf{E}||a$ and (b) $\mathbf{E}||b$ (pressure medium: argon). Insets: Frequency of orbital excitations as a function of temperature. Lines are guides to the eye.

superstructure.⁵ An additional, second-order phase transition is found at $T_{c2}=47$ K, where the material changes from the intermediate phase to the one-dimensional antiferromagnetic phase at high temperature.

Starting from room temperature and low-pressure (0.8 GPa) conditions, transmittance measurements on TiOBr were carried out upon temperature decrease. Fig. 6 shows the temperature-dependent transmittance spectra for the polarizations $\mathbf{E}||a$ and $\mathbf{E}||b$. The oscillations in the spectra are Fabry-Perot resonances due to multiple reflections within the thin sample platelet. With decreasing temperature one notices a small but significant shift of the orbital excitations to higher frequencies, as illustrated in the insets of Fig. 6. The most pronounced changes occur between 295 and 200 K and can be attributed to the thermal contraction of the lattice while cooling down, leading to a smaller volume of the TiO_4Br_2 octahedra and thus to a stronger crystal field.²⁰ Below 100 K the orbital excitations hardly shift with temperature, which suggests that the structural changes occurring at the phase transitions at $T_{c1}=27$ K and $T_{c2}=47$ K have only a small effect on the TiO_4Br_2

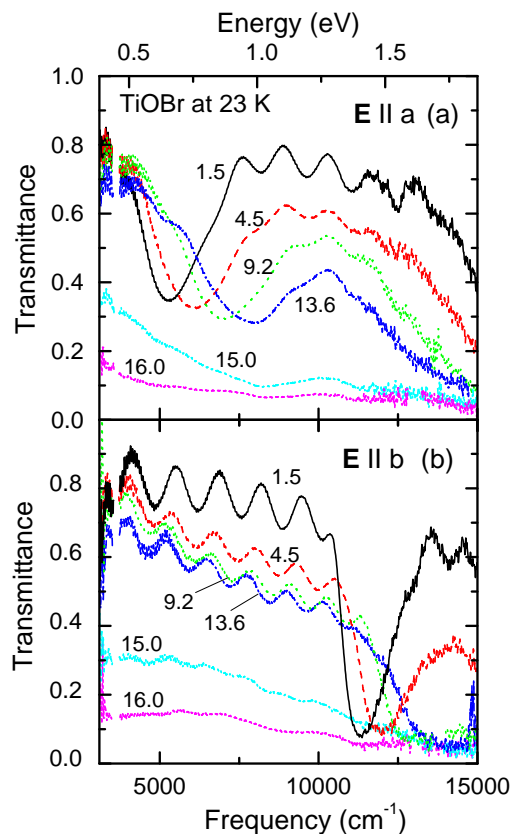


FIG. 7: (Color online) Transmittance $T(\omega)=I_s(\omega)/I_r(\omega)$ (see text for definitions) of TiOBr as a function of pressure at 23 K, for the polarization (a) $\mathbf{E}||a$ and (b) $\mathbf{E}||b$ (pressure medium: argon).

octahedra and hence on the crystal field. This in agreement with an earlier work showing that the orbital degree of freedom is irrelevant for the low-energy physics, in particular the exotic spin-Peierls behavior with two successive phase transitions.⁶

At 23 K, where the sample is in the spin-Peierls state for ambient pressure, transmittance spectra were recorded for several pressures (see Fig. 7). Similar to the room-temperature results, the transmittance is suppressed over the whole studied frequency range above a certain pressure; however, at 23 K the suppression occurs only above ≈ 16 GPa, compared to the room-temperature transition pressure of 14 GPa.

We also followed the pressure-induced shifts of the orbital excitations at 23 K [Figs. 3 (c) and (d)]. With increasing pressure the frequencies of the orbital excitations increase linearly with increasing pressure. Like for the room-temperature results, we relate this shift to a pressure-induced decrease of the octahedral volume and a possible change in octahedral distortion, causing a change in the crystal field (see Sec. III A). At room-temperature we noticed a small difference in the frequencies of the orbital excitations for pressure increase and decrease. This difference is much more pronounced at

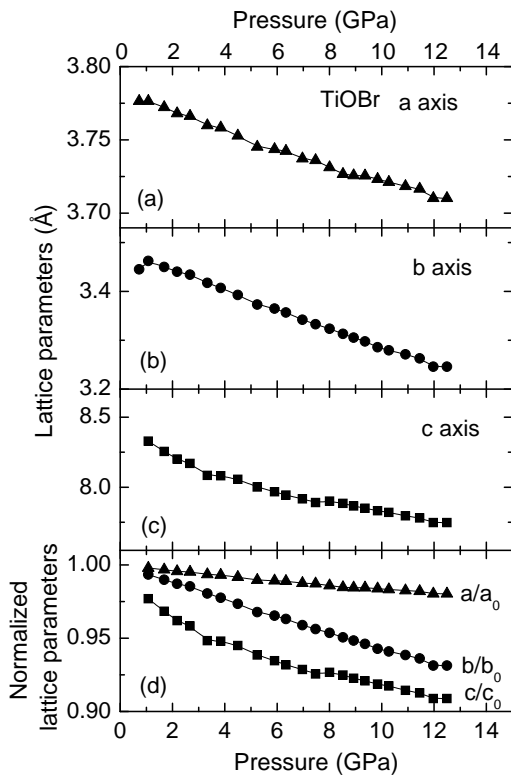


FIG. 8: (Color online) Lattice parameters of TiOBr at room temperature as a function of pressure (pressure medium: helium). (a)-(c) Lattice parameters a , b , c . (d) Lattice parameters a , b , c normalized to their respective zero-pressure values. Lines are guides to the eye.

23 K. For example, for $\mathbf{E}||a$ already at around 4 GPa during pressure release the ambient-pressure excitation energy of $\approx 5370 \text{ cm}^{-1}$, and thus the ambient-pressure crystal field strength, has been reached [see Fig. 3(c)].

C. Pressure-induced structural phase transition at room temperature

For the understanding of the drastic changes in the optical response under pressure, we carried out x-ray powder diffraction measurements on TiOBr and TiOCl at room temperature as a function of pressure. A typical diffraction pattern (not shown) does not consist of concentric rings as expected for powder diffraction data, but it contains separate spots. This is due to the fact that it was not possible to produce good TiOX powders with homogenous grain size distributions and random orientations because of the platelet-like habits and the softnesses of the crystallites. Instead, the crystallites inside the DAC orient their c crystal axis preferentially perpendicular to the diamond anvil surface, i.e., along the direction of incidence of the x-radiation. Therefore, Rietveld refinements of the diffraction patterns could not be carried out. Nevertheless LeBail fits of the diffraction

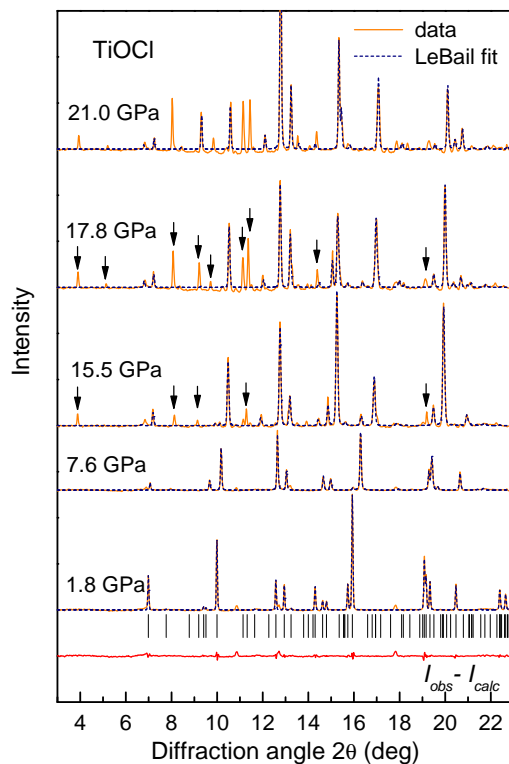


FIG. 9: (Color online) Room-temperature x-ray powder diffraction diagrams of TiOCl at high pressures ($\lambda = 0.4128 \text{ \AA}$) together with the LeBail fits (pressure medium: helium). For the lowest applied pressure (1.8 GPa) the difference curve ($I_{obs} - I_{calc}$) between the diffraction diagram and the LeBail fit is shown. Markers show the calculated peak positions for the ambient-pressure phase. Above 15.5 GPa the diffraction diagram can no longer be described by the ambient-pressure crystal symmetry. Arrows indicate the diffraction peaks with the most obvious discrepancy between the data and the LeBail fitting curve.

patterns could be accomplished, in order to determine the unit cell volume and the lattice parameters as a function of pressure.

The room-temperature diffraction diagrams of TiOBr can be well fitted with the ambient-pressure crystal structure (space group $Pmmn$) at low pressures, as demonstrated in Ref.8. The lattice parameters of TiOBr as a function of pressure, as obtained from the LeBail fitting, are presented in Fig. 8. The changes of the lattice parameters a and b with pressure are linear over a large pressure range. The behavior of the lattice parameters c rather follows a sublinear fashion. In Fig. 8 we also show the lattice parameters a , b , c normalized to their respective zero-pressure values as a function of pressure [Fig. 8 (d)]. According to these results, TiOBr has a very anisotropic compressibility, with the largest compressibility along the c axis, i.e., the stacking axis of the buckled Ti-O bilayers.

At around 14 GPa the diffraction diagram of TiOBr undergoes pronounced changes and is no longer com-

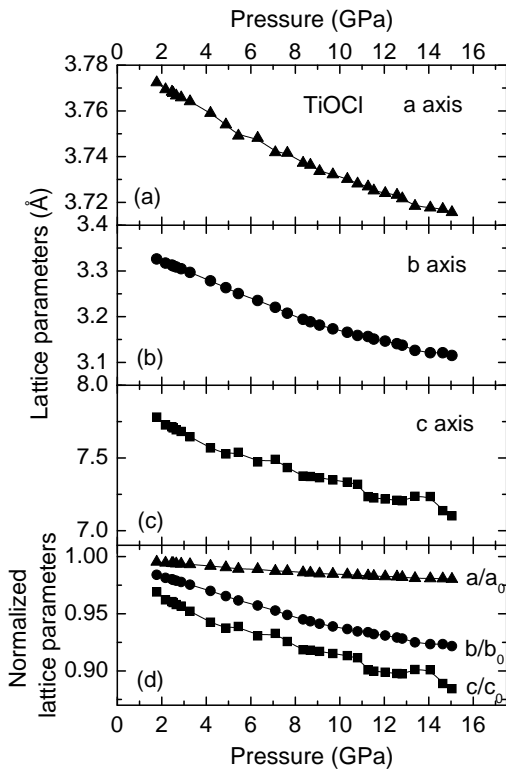


FIG. 10: (Color online) Lattice parameters of TiOCl at room temperature as a function of pressure (pressure medium: helium). (a)-(c) Lattice parameters a , b , c . (d) Lattice parameters a , b , c normalized to their respective zero-pressure values. Lines are guides to the eye.

patible with the ambient-pressure crystal structure symmetry.⁸ We can therefore conclude that TiOBr undergoes a structural phase transition at 14 GPa.

We also include the corresponding results from the pressure-dependent x-ray powder diffraction on TiOCl, namely the room-temperature diffraction diagrams for selected pressures together with the LeBail fits (Fig. 9) as well as the lattice parameters as a function of pressure extracted by the LeBail fits (Fig. 10). The sublinear dependence on pressure is obvious for all three lattice parameters. Pronounced changes of the diffraction diagram occur at 15.5 GPa indicating a pressure-induced structural phase transition in TiOCl, similar like in TiOBr. For both compounds the pressure-induced changes are reversible in terms of the positions of the diffraction peaks.

From the lattice parameters the pressure dependence of the unit cell volume V for both compounds was obtained. In Fig. 11 we plot $V(p)$ together with a fit according to the Murnaghan equation²²

$$V(p) = V_0[(B'/B_0)p + 1]^{-1/B'} \quad (3)$$

with the bulk modulus $B_0 = -dp/d\ln V$ and its derivative B' at zero pressure. The ambient-pressure unit cell volume V_0 was kept fixed at the experimental value of $112.4(5) \text{ \AA}^3$ [$102.7(6) \text{ \AA}^3$] for TiOBr (TiOCl).¹⁹ The bulk

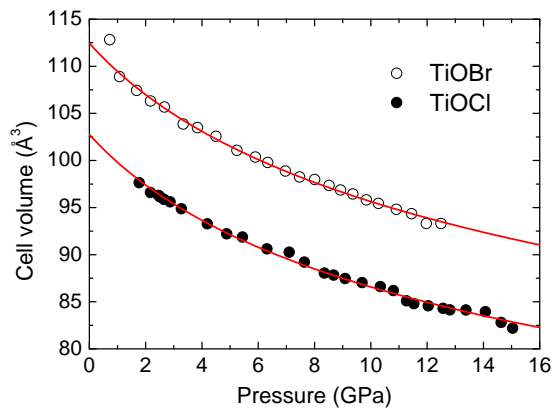


FIG. 11: (Color online) Unit cell volume V of TiOCl and TiOBr as a function of pressure P . The full, red (gray) lines are fits according to Eq. (3).

moduli B_0 evaluated according to the Murnaghan equation are 33.7 ± 0.8 GPa and 31.0 ± 0.9 GPa for TiOBr and TiOCl, and the derivatives B' are 6.9 ± 0.3 and 6.7 ± 0.3 , respectively. The bulk modulus of TiOBr is slightly larger than that of TiOCl, i.e., TiOBr is slightly less compressible than TiOCl. Furthermore, one notices that the pressure derivative B' of both compounds is significantly larger compared to the value $B' \approx 4$ typically found for three-dimensional solids with isotropic elastic properties. The enhanced value of B' thus suggests anisotropic compression properties of TiOX. It is interesting to note that the bulk modulus B_0 and its derivative B' of TiOX are close to the corresponding values found for graphite ($B_0=33.8$ GPa, $B'=8.9$).²³

IV. DISCUSSION

A. Comparison of transition pressures: TiOBr and TiOCl

In Table I we compare the transition pressures of TiOBr and TiOCl at room temperature obtained by different experimental techniques (transmittance, reflectance, x-ray powder diffraction) and for different pressure media. First, comparing the corresponding results for the two compounds, one notices a pressure difference of ≈ 2 GPa. This suggests the existence of some sort of chemical pressure effect in TiOX.

A starting point for the understanding of this finding could be a comparison of the ambient-pressure lattice parameters. The lattice parameters b and c of TiOBr ($a=3.785$ Å, $b=3.485$ Å, $c=8.525$ Å) are significantly larger than those of TiOCl ($a=3.789$ Å, $b=3.365$ Å, $c=8.060$ Å).^{2,19} The difference is most pronounced for the c axis; here, the larger value in TiOBr can be attributed to the larger size of the Br⁻ ions, which form layers separating the buckled Ti-O bilayers. Naively, one would then expect a *higher* pressure to induce the transition in

TABLE I: Comparison of transition pressures of TiOCl and TiOBr at room temperature obtained from transmittance, reflectance, and x-ray powder diffraction measurements for different pressure transmitting media.

material	transmittance (CsI)	transmittance (argon)	transmittance (alcohol mixture)	reflectance (CsI)	x-ray diffraction (helium)
TiOCl	12 GPa	16 GPa	≈ 16 GPa	12 GPa	15.5 GPa
TiOBr	10-11 GPa	14 GPa (295 K) 16 GPa (23 K)	not measured	10-11 GPa	14 GPa

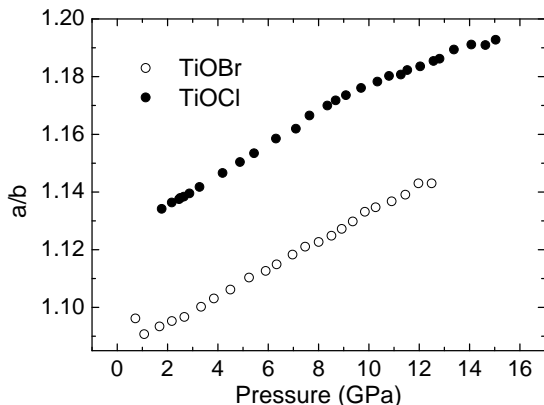


FIG. 12: Pressure-dependent ratio of the lattice parameters a and b for the TiOBr and TiOCl at room temperature. The ratio a/b as a function of pressure follows a linear behavior.

TiOBr compared to TiOCl, which is in contradiction to our findings. Thus, not the distance between the Ti-O bilayers but the pressure-induced crystal structure changes *within* the bilayers seem to be the crucial parameter for inducing the closure of the Mott-Hubbard gap in TiOX. This furthermore suggests that the high-pressure phase has a dimensionality of less than three, being mainly confined to the buckled Ti-O bilayers.

A two-dimensional character of the high-pressure phase could indeed explain the difference in the critical pressures for TiOBr and TiOCl: At ambient conditions the one-dimensional character of TiOBr is weaker than in TiOCl, since the lattice parameter ratio (a/b) in TiOBr ($a/b=1.086$) is smaller than in TiOCl ($a/b=1.126$).¹⁹ This is consistent with magnetic susceptibility measurements showing a larger deviation from the Bonner-Fisher type behavior above the spin-Peierls transition for TiOBr compared to TiOCl.²⁰ The more two-dimensional character of TiOBr was also demonstrated by recent photoemission experiments and supported by density-functional calculations.²⁴ Hence, in the case of TiOBr less pressure would be needed to drive the system into a (prospective) two-dimensional, high-pressure phase.

Our pressure-dependent crystal structure data can provide a test of this picture (two-dimensional character of the high-pressure phase): In Fig. 12 we plot the ratio a/b for both studied compounds as a function of pressure. This ratio should decrease towards the value 1

under pressure in the case of a two-dimensional high-pressure phase. Instead, the ratio a/b *increases* with increasing pressure for both compounds: TiOBr and TiOCl become more one-dimensional under pressure. Obviously, a different criterium regarding the changes of the crystal structure with applied pressure has to be used, in order to explain the difference of ≈ 2 GPa for the critical pressures of TiOBr and TiOCl. At this point we can only speculate about possible criteria for the Mott-Hubbard gap closure – like a critical Ti-Ti distance along b or a direction – since information about the shifts of the atomic coordinates under pressure is not available.

B. Mott-Hubbard gap closure and structural phase transition

Under hydrostatic conditions, i.e., for argon as pressure medium, the closure of the Mott-Hubbard gap in TiOBr (TiOCl) occurs at 14 GPa (16 GPa) (Table I). Under less hydrostatic conditions, i.e., using CsI as pressure medium, the gap closure happens at somewhat lower pressure ($\Delta P \approx 4$ GPa). This offset in the transition pressure for different types of pressure media has been reported earlier for TiOCl and LaTiO_{3.41}.^{7,15} The important finding is that under similar hydrostatic conditions the closure of the Mott-Hubbard gap in TiOX coincides with a structural phase transition, as demonstrated by our pressure-dependent x-ray powder diffraction data (Table I). Therefore, the gap closure in TiOX is not of purely electrical origin, but the lattice degree of freedom has to be taken into account too.

In this regard it is interesting to compare the results for TiOBr and TiOCl with typical examples of bandwidth-controlled Mott transitions under external pressure, which are discussed in literature. One finds the general observation that the Mott transition coincides with volume discontinuities or even changes of the crystal symmetry. This applies, for example, to the canonical Mott-Hubbard systems VO₂ (Ref.25) and vanadium sesquioxide doped with chromium, (V_{0.95}Cr_{0.04})₂O₃,^{26,27,28} and also to MnO,²⁹ YNiO₃,³⁰ Fe₂O₃,³¹ or FeI₂.³² It was even suggested that as a rule the Mott transition coincides with a structural phase transition and volume collapse.³² Our finding of a pressure-induced structural phase transition in TiOBr and TiOCl at the same pressure where the Mott-Hubbard gap closes, is in agreement with such

an interpretation of the Mott-Hubbard transition.

The importance of electronic correlations for the underlying mechanism of the observed gap closure in TiOX is suggested by the effective mass of the charge carriers, as estimated from the spectral weight analysis. As demonstrated in Sec. III A, for both TiOBr and TiOCl the spectral weight becomes pressure-independent above a certain pressure [see inset of Fig. 5 and Fig. 4(b) in Ref.7]. From the high-pressure value of the spectral weight one can estimate an effective density of charge carriers according to Eq. (2),³³ averaged over the two studied crystal directions, to $n_{eff}=(0.6 \pm 0.2) \cdot 10^{21} \text{cm}^{-3}$ for TiOBr and $n_{eff}=(1.3 \pm 0.2) \cdot 10^{21} \text{cm}^{-3}$ for TiOCl for the same frequency range.⁷ Based on these values the effective number of charge carriers per Ti atom, N_{eff} , can in principle be calculated, if the unit cell volume and the number of formula units per unit cell are known. For an estimate of N_{eff} we assumed a high-pressure volume of 93 \AA^3 (82 \AA^3) and a number of formula units per unit cell of $Z=2$ ($Z=2$) for TiOBr (TiOCl). Hereby, we neglected the change of the crystal symmetry and a possible collapse of the unit cell volume at the insulator-to-metal transition; the latter effect usually ranges between 1 and 10 %.^{26,29,31,32} Under these assumptions we obtained $N_{eff}=0.03 \pm 0.01$ for TiOBr and $N_{eff}=0.05 \pm 0.01$ in the case of TiOCl. I. e., N_{eff} is much lower than the expected value of 1.

One possible explanation for the reduced value of N_{eff} could be that the charge carriers only partly contribute to the excitations in the specified frequency range. In addition, the reduction might be related to an enhanced effective mass of the charge carriers, typically found in materials with strong electronic correlations. The mass enhancement in TiOX might get stronger when the system approaches the Mott insulating state, as suggested by the suppressed carrier density with decreasing pressure [see inset of Fig. 5 and Fig. 4(b) in Ref.7]. A mass enhancement in the vicinity of a transition to a Mott insulator was theoretically predicted³⁴ and observed in some cases.^{35,36}

In order to understand the main mechanism driving the observed closure of the Mott-Hubbard gap, the crystal structure of the high-pressure phase might be an important piece of information. However, up to now we could not resolve the symmetry of the crystal structure at high pressures. In this regard, density-functional calculations³⁷ might provide predictions which could then be tested on our x-ray diffraction data.

Finally, we would like to comment on the possibility of the metallic character of the high-pressure phase in TiOX. Based on our data we cannot prove the existence of a Drude term in the optical response related to coherent quasiparticles at high pressures.³⁸ It was, however, demonstrated theoretically and experimentally in various cases, that above a certain temperature the absence of a Drude term in a correlated system located on the metallic side of the Mott transition is to be expected: A lot of theoretical work has been devoted to the

transport properties of systems close to the first-order Mott transition at low temperatures and in the crossover regime at elevated temperatures. Optical conductivity spectra for different interaction strengths and different temperatures were obtained in a dynamical mean-field theory (DMFT) treatment of the Hubbard model.³⁹ It was shown that only below a certain temperature T_{coh} a quasiparticle peak involving coherent excitations appears at the Fermi energy and the Fermi liquid description applies. As a result, only at low temperatures ($T < T_{coh}$) a Drude term should be present in the optical conductivity spectrum. With increasing temperature, the quasiparticle peak is gradually destroyed and disappears above the temperature T_{coh} . Such a behavior was demonstrated for the two-dimensional organic charge-transfer salts κ -(BEDT-TTF)₂Cu[N(CN)₂]Br_xCl_{1-x}.³⁶ Even for a high Br content, i.e., on the metallic side of the Mott transition, no Drude-like peak is present down to approx. 50 K. Only below this temperature a Drude-like feature appears, which can be described with an extended Drude model, with a frequency-dependent scattering rate and effective mass.

The optical conductivity spectra of TiOX as a function of pressure were obtained at room temperature. According to the findings for organic salts mentioned above and in other cases,³⁹ the seeming absence of a Drude-like contribution in the optical response of TiOX at high pressures could be explained by the elevated measurement temperature. Still, the metallic state appears to be the most plausible high-pressure phase for TiOX based on our experimental results. The shape of the optical conductivity spectra at high pressures is, however, an open issue. Furthermore, a direct proof of the Drude response might be obtainable by pressure-dependent reflectance measurements carried out at low temperatures.

V. CONCLUSIONS

In conclusion, we have studied the pressure-dependent optical response of TiOBr and TiOCl at room temperature by transmittance and reflectance measurements in combination with pressure-dependent x-ray powder diffraction experiments. For both compounds the infrared transmittance is suppressed above a critical pressure. The pressure-dependent reflectance and corresponding optical conductivity spectra reveal additional electronic excitations at high pressures extending down to the far-infrared range. These findings suggest the closure of the Mott-Hubbard gap under pressure. For TiOBr the pressure-induced suppression of the infrared transmittance also occurs at 23 K, where the compounds is in the spin-Peierls phase at ambient pressure. The orbital excitations in TiOBr shift linearly to higher frequency with increasing pressure. The shifts are not completely reversible upon pressure release, especially at low temperatures.

The pressure-induced changes occur at somewhat lower

pressure in the case of TiOBr compared to TiOCl. This difference cannot be attributed to the more two-dimensional character of TiOBr, since according to the ratio of the crystal parameters a and b the system becomes more one-dimensional under pressure, i.e., the high-pressure state seems to be rather of one-dimensional than of two-dimensional character.

The closure of the Mott-Hubbard gap coincides with a structural phase transition. From the results of our pressure-dependent x-ray powder diffraction measurements on TiOBr and TiOCl we could furthermore extract the pressure-dependence of the lattice parameters and of the unit cell volume. The latter can be well described by the Murnaghan equation. The enhancement of the effective mass of the charge carriers around the critical pressure suggests the importance of electronic correlations for the mechanism driving the transition. However, the lattice degree of freedom seems to play an important role as well, since the crystal symmetry changes at the

transition pressure.

Acknowledgements

We acknowledge the ANKA Angströmquelle Karlsruhe for the provision of beamtime and we would like to thank B. Gasharova, Y.-L. Mathis, D. Moss, and M. Süpfle for assistance using the beamline ANKA-IR. Facilities and beamtime provided by the European Synchrotron Radiation Facility is gratefully acknowledged. We furthermore thank K. Syassen for providing valuable information about the optical design of the infrared microscope with large working distance. Fruitful discussions with Jan Kunes are gratefully acknowledged. Financial support by the DFG, including the Emmy Noether-program, SFB 484, and DFG-CL124/6-1, is acknowledged.

-
- * E-mail: christine.kuntscher@physik.uni-augsburg.de
- ¹ A. Seidel, C. A. Marianetti, F. C. Chou, B. Ceder, and P. A. Lee, *Phys. Rev. B* **67**, 020405 (2003).
 - ² V. Kataev, J. Baier, A. Möller, L. Jongen, G. Meyer, and A. Freimuth, *Phys. Rev. B* **68**, 140405 (R) (2003).
 - ³ G. Caimi, L. Degiorgi, N. N. Kovaleva, P. Lemmens, and F. C. Chou, *Phys. Rev. B* **69**, 125108 (2004).
 - ⁴ M. Shaz, S. van Smaalen, L. Palatinus, M. Hoinkis, M. Klemm, S. Horn, and R. Claessen, *Phys. Rev. B* **71**, 100405 (2005).
 - ⁵ S. van Smaalen, L. Palatinus, and A. Schönleber, *Phys. Rev. B* **72**, 020105(R) (2005).
 - ⁶ R. Rückamp, J. Baier, M. Kriener, M. W. Haverkort, T. Lorenz, G. S. Uhrig, L. Jongen, A. Möller, G. Meyer, and M. Grüninger, *Phys. Rev. Lett.* **95**, 097203 (2005).
 - ⁷ C. A. Kuntscher, S. Frank, A. Pashkin, M. Hoinkis, M. Klemm, M. Sing, S. Horn, and R. Claessen, *Phys. Rev. B* **74**, 184402 (2006).
 - ⁸ C. A. Kuntscher, S. Frank, A. Pashkin, H. Hoffmann, A. Schönleber, S. van Smaalen, M. Hanfland, S. Glawion, M. Klemm, M. Sing, S. Horn and R. Claessen, *Phys. Rev. B* **76**, 241101(R) (2007).
 - ⁹ R. J. Beynon and J. A. Wilson, *J. Phys.: Condens. Matter* **5**, 1983 (1993).
 - ¹⁰ L. Craco, M. S. Laad, and E. Müller-Hartmann, *J. Phys.: Condens. Matter* **18**, 10943 (2006); arXiv:cond-mat/0410472.
 - ¹¹ W. Gaebel, M. Klemm, C. A. Kuntscher, A. Pashkin, H. Hoffmann, and S. Horn, unpublished.
 - ¹² H. Schäfer, F. Wartenpfehl, and E. Weise, *Z. Anorg. Allg. Chem.* **295**, 268 (1958).
 - ¹³ H. G. von Schnering, M. Collin, and M. Hassheider, *Z. Anorg. Allg. Chem.* **387**, 137 (1972).
 - ¹⁴ H. K. Mao, J. Xu, and P.M. Bell, *J. Geophys. Res.* **91**, 4673 (1986).
 - ¹⁵ S. Frank, C. A. Kuntscher, I. Loa, K. Syassen, and F. Lichtenberg, *Phys. Rev. B* **74**, 054105 (2006).
 - ¹⁶ G. Huber, K. Syassen, and W. B. Holzapfel, *Phys. Rev. B* **15**, 5123 (1977).
 - ¹⁷ A. Hammersley, computer program FIT2D (ESRF, Grenoble, 1998).
 - ¹⁸ V. Petricek, M. Dusek, and L. Palatinus. Jana2000. A crystallographic computing system. Institute of Physics, Praha, Czech Republic (2006).
 - ¹⁹ T. Sasaki, M. Mizumaki, K. Kato, Y. Watabe, Y. Nishihata, M. Takata, and J. Akimitsu, *J. Phys. Soc. Jpn.* **74**, 2185 (2005).
 - ²⁰ C. Kato, Y. Kobayashi, and M. Sato, *J. Phys. Soc. Jpn.* **74**, 473 (2005).
 - ²¹ G. Caimi, L. Degiorgi, P. Lemmens, and F. C. Chou, *J. Phys.: Condens. Matter* **16**, 5583 (2004).
 - ²² F. D. Murnaghan, *Proc. Natl. Acad. Sci.* **30**, 244 (1944).
 - ²³ M. Hanfland, H. Beister, and K. Syassen, *Phys. Rev. B* **39**, 12598 (1989).
 - ²⁴ M. Hoinkis, M. Sing, S. Glawion, L. Pisani, R. Valenti, S. van Smaalen, M. Klemm, S. Horn, and R. Claessen, *Phys. Rev. B* **75**, 245124 (2007).
 - ²⁵ E. Arcangeletti, L. Baldassarre, D. Di Castro, S. Lupi, L. Malavasi, C. Marini, A. Perucchi, and P. Postorino, *Phys. Rev. Lett.* **98**, 196406 (2007).
 - ²⁶ D. B. McWhan and J. P. Remeika, *Phys. Rev. B* **2**, 3734 (1970).
 - ²⁷ D. B. McWhan, J. P. Remeika, T. M. Rice, W. F. Brinkman, J. P. Maita, and A. Menth, *Phys. Rev. Lett.* **27**, 941 (1971).
 - ²⁸ D. B. McWhan, A. Menth, J. P. Remeika, W. F. Brinkman, and T. M. Rice, *Phys. Rev. B* **7**, 1920 (1973).
 - ²⁹ C. S. Yoo, B. Maddox, J.-H. P. Klepeis, V. Iota, W. Evans, A. McMahan, M. Y. Hu, P. Chow, M. Somayazulu, D. Häusermann, R. T. Scalettar, and W. E. Pickett, *Phys. Rev. Lett.* **94**, 115502 (2005).
 - ³⁰ J. L. Garcia-Munoz, M. Amboage, M. Hanfland, J. A. Alonso, M. J. Martinez-Lope, and R. Mortimer, *High Pressure Research*, **23**, 171 (2003).
 - ³¹ G. Kh. Rozenberg, L. S. Dubrovinsky, M. P. Pasternak, O. Naaman, T. Le Bihan, and R. Ahuja, *Phys. Rev. B* **65**, 064112 (2002).
 - ³² G. Kh. Rozenberg, M. P. Pasternak, W. M. Xu, L. S.

- Dubrovinsky, J. M. Osorio Guillen, R. Ahuja, B. Johansson, and T. Le Bihan, Phys. Rev. B **68**, 064105 (2003).
- ³³ For the estimation of the effective carrier density n_{eff} we used the free electron mass. Furthermore, we assumed a background dielectric constant $\epsilon_{\infty} \approx 3$ in the Drude-Lorentz fitting, as described in Sec. III A.
- ³⁴ W. F. Brinkman and T. M. Rice, Phys. Rev. B **2**, 4302 (1970).
- ³⁵ M. M. Qazilbash, K. S. Burch, D. Whisler, D. Shrenkhamer, B. G. Chae, H. T. Kim, and D. N. Basov, Phys. Rev. B **74**, 205118 (2006).
- ³⁶ J. Merino, M. Dumm, N. Drichko, M. Dressel, and Ross H. McKenzie, Phys. Rev. Lett. **100**, 086404 (2008).
- ³⁷ Y.Z. Zhang, H.O. Jeschke, and R. Valenti, in preparation.
- ³⁸ M. J. Rozenberg, G. Kotliar, H. Kajueter, G. A. Thomas, D. H. Rapkine, J. M. Honig, and P. Metcalf, Phys. Rev. Lett. **75**, 105 (1995).
- ³⁹ See, for example, A. Georges, G. Kotliar, W. Krauth, and M. J. Rozenberg, Rev. Mod. Phys. **68**, 13 (1996); M. J. Rozenberg, T. Kotliar, H. Kajueter, G. A. Thomas, D. H. Rapkine, J. M. Honig, and P. Metcalf, Phys. Rev. Lett. **75**, 105 (1995); J. Merino and R. H. McKenzie, Phys. Rev. B **61**, 7996 (2000).